Weierstraß-Institut

für Angewandte Analysis und Stochastik

Leibniz-Institut im Forschungsverbund Berlin e. V.

Preprint ISSN 2198-5855

Transport of solvated ions in nanopores: Asymptotic models and numerical study

Jürgen Fuhrmann[1], Clemens Guhlke[1], Bartlomiej Matejczyk[2], Rüdiger Müller[1]

submitted: July 30, 2018

[1] Weierstrass Institute
Mohrenstr. 39
10117 Berlin
Germany
E-Mail: juergen.fuhrmann@wias-berlin.de
clemens.guhlke@wias-berlin.de
ruediger.mueller@wias-berlin.de

[2] Department of Mathematics
University of Warwick
CV4 7AL Coventry
United Kingdom
E-Mail: b.matejczyk@warwick.ac.uk

No. 2526
Berlin 2018

2010 *Mathematics Subject Classification.* 35C20, 65-05, 78A57.

Key words and phrases. Nanopore, electro-thermodynamics, ion transport, finite ion size, solvation.

The authors gratefully acknowledge support by the Einstein Foundation Berlin with in the MATHEON Project CH11 "Sensing with Nanopores".

Edited by
Weierstraß-Institut für Angewandte Analysis und Stochastik (WIAS)
Leibniz-Institut im Forschungsverbund Berlin e. V.
Mohrenstraße 39
10117 Berlin
Germany

Fax: +49 30 20372-303
E-Mail: preprint@wias-berlin.de
World Wide Web: http://www.wias-berlin.de/

Transport of solvated ions in nanopores: Asymptotic models and numerical study

Jürgen Fuhrmann, Clemens Guhlke, Bartlomiej Matejczyk, Rüdiger Müller

Abstract

Improved Poisson–Nernst–Planck systems taking into account finite ion size and solvation effects provide a more accurate model of electric double layers compared to the classical setting. We introduce and discuss several variants of such improved models. We study the effect of improved modeling in large aspect ratio nanopores. Moreover, we derive approximate asymptotic models for the improved Poisson–Nernst–Planck systems which can be reduced to one-dimensional systems. In a numerical study, we compare simulation results obtained from solution of the asymptotic 1D-models with those obtained by discretization of the full resolution models.

1 Introduction

Artificial nanopores gained attention as an attractive technology for low cost/high speed sensing of macromolecules [HS09, Key11]. Further optimization of this technology requires accurate characterization of the pore material properties and a better understanding of the ion transport and flow behavior. Due to their size, experimental investigations are hard to undertake. Thus, mathematical modeling and simulation are crucial to gain a detailed understanding of flow and transport in nanopores. But also numerical simulation is complicated because of strong nonlinearities, the very short width of the occurring boundary layers which requires very fine grids for the discretization, and the large aspect ratio of the geometry.

Surface charges on the inner pore walls are compensated by counter ion accumulation, leading to the formation of the so called electrical double layer. The Debye length that characterizes the width of the double layer typical is in the range of a few nanometers, and therefore it is in the same order of magnitude as the width of the narrowest parts of the nanopore itself. As the double layer amounts for large part of the volume inside a pore, the consistent incorporation of its structure into the models is mandatory. The classical Poisson–Nernst–Planck (PNP) theory fails to provide such a model. It typically overestimates the stored charge in the double layer by several orders of magnitude because it is based on the assumption of strongly diluted solutions and therefore ignores volume exclusion, ion–solvent interaction and coupling to the momentum balance. Improved models for electrolytes in this respect have been discussed e.g. in [Bik42, BAO97, KBA07, BSW12]. Recently, improved models of electrolytes and electrochemical interfaces have been consistently derived from first principles of on non-equilibrium thermodynamics [DGM13, DGL14, DGM18].

Asymptotic models can take advantage of the strongly anisotropic character of the pore geometry and allow the reduction to spatially one-dimensional systems which can be solved with significantly less computational cost. In spite of its well known deficiencies, PNP theory is used in most of the available research on nanopores, cf. e.g. [SAB$^+$03, CSP05, CS07, VSS08], and also for the even smaller biological ion channels, cf. e.g. [CKC00, YVS$^+$05, ZW11]. Asymptotic analysis based on PNP models has been applied e.g. in [SGNE08, SN09] and compared to experimental data. For the

DOI 10.20347/WIAS.PREPRINT.2526 Berlin 2018

asymptotic analysis of classical PNP equations which includes rotational effects see [MPWR18], where approximate solution based on solving the Poisson-Boltzmann equation in different regimes is proposed. Also models that take steric effects into account have been applied for ion channels and nanopores, cf. [CGMP03, HLLE12, BSW12, CCAO14].

In this paper we derive asymptotic models for improved Nernst–Planck systems, taking into account finite ion size and solvation effects under the assumption of mechanical equilibrium. Moreover, we describe a way how the spatial dimension of the asymptotic model can be reduced to a truly one-dimensional system by applying exact solution to the asymptotic approximate equations in one direction. Our numerical study is influenced by the geometry of typical polyethylene terepthalate (PET) nanopores, which are produced by irradiating a 12μm thick PET foil with heavy ions and subsequent chemical etching which results in a radially symmetric pore. Here, we focus on a a different simplification of the domain that assumes planar symmetry.

Outline. First, in Sect. 2 we discuss a general form of continuum models for electrolyte transport and present different material models from the literature. Next, in Sect. 3 we state details of the geometry and the physical parameters of the nanopores. In Sect. 4 we present the dimensionless form of the model equations and derive an asymptotic model together with a reduction to a 1D system. The numerical study is reported in Sect. 5 covering two different types of nanopores as well as discussion of different solvation models. We end with some conclusions in Sect. 6.

2 Ion transport in liquid electrolytes and application to nanopores

The electrolyte is modeled as a mixture of $N+1$ constituents. For referencing the individual constituents we use the index set $\mathcal{I} = \{1, 2, \cdots, N, S\}$ For a description on a continuum level, each of the constituents is characterized by the (atomic) mass m_α and its atomic charge $z_\alpha e_0$, where the positive constant e_0 is the elementary charge and z_α is the charge number of the constituent. We will always assume that the solvent is neutral, i.e. $z_S = 0$.

Basic quantities. The electrolytic mixture occupies a region $\Omega \subset \mathbb{R}^3$. At any time t, the thermodynamic state of Ω in an isothermal, incompressible and electrostatic setting is described by number densities n_α for $\alpha \in \mathcal{I}$, barycentric velocity $\boldsymbol{v}$, pressure p and electric potential φ. The introduced quantities may be functions of time t and space $x = (x^1, x^2, x^3) \in \Omega$.

Multiplication of the number densities n_α by the masses m_α gives the partial mass densities,

$$\rho_\alpha = m_\alpha n_\alpha \, . \tag{2.1}$$

The summation over the partial mass densities, number densities and products of number densities and charges defines the (total) mass density, total number density and the free charge density, respectively,

$$\rho = \sum_{\alpha\in\mathcal{I}} \rho_\alpha \, , \qquad n = \sum_{\alpha\in\mathcal{I}} n_\alpha \, , \qquad n^{\mathrm{F}} = \sum_{\alpha\in\mathcal{I}} z_\alpha e_0 n_\alpha \, . \tag{2.2}$$

For the later representation of the constitutive equation we introduce the mole fractions,

$$y_\alpha = \frac{n_\alpha}{n} \qquad \Longrightarrow \qquad 1 = \sum_{\alpha\in\mathcal{I}} y_\alpha \, . \tag{2.3}$$

Balance equations of mass, momentum and Poisson equation. In the electrostatic approximation of Maxwell's equations the magnetic contributions vanishes and only the electric field $\boldsymbol{E} = -\nabla\varphi$ remains. The coupled system of equations for the basic variables then relies on balance equations of partial masses and momentum, and the Poisson equation for the electric potential. The mass densities ρ_α, resp. number densities n_α, the barycentric velocity $\boldsymbol{v}$ and the potential φ satisfy

$$-\operatorname{div}((1+\chi)\varepsilon_0\nabla\varphi) = n^{\mathrm{F}}\,, \tag{2.4a}$$

$$\partial_t\rho_\alpha + \operatorname{div}(\rho_\alpha\boldsymbol{v} + \boldsymbol{J}_\alpha) = r_\alpha\,, \qquad \text{for } \alpha\in\mathcal{I}\,, \tag{2.4b}$$

$$\partial_t\rho\boldsymbol{v} + \operatorname{div}(\rho\boldsymbol{v}\otimes\boldsymbol{v} - \boldsymbol{\Sigma}) = \rho\boldsymbol{b}\,. \tag{2.4c}$$

Here, $\boldsymbol{J}_\alpha$ are the non-convective mass fluxes, r_α are the production rates due to chemical reactions, $\boldsymbol{\Sigma}$ is the total stress tensor[1], and $\rho\boldsymbol{b}$ is the force density due to gravitation. Moreover, ε_0 is the dielectric constant and χ is the constant dielectric susceptibility of the mixture.

General constitutive equations for liquid electrolytes. The balance equations have to be complemented by constitutive equations for the mass fluxes $\boldsymbol{J}_\alpha$ and the total stress tensor $\boldsymbol{\Sigma}$. The constitutive equations are not uniquely determined, thus there is some freedom in the modeling. Nevertheless the constitutive modeling is restricted by the second law of thermodynamics and symmetry principles and we refer to [Mül85, BD15, DGM18] for the general strategy of constitutive modeling in the contexts of (electro-) thermodynamics.

First of all we note that the mass fluxes are not independent of each other, but they are restricted by the constraint

$$\sum_{\alpha\in\mathcal{I}}\boldsymbol{J}_\alpha = 0\,. \tag{2.5}$$

The general constitutive equations in an isothermal, electrostatic setting read

$$\boldsymbol{J}_\alpha = -\sum_{\beta=1}^{N} D_{\alpha\beta}\tfrac{\rho_\beta}{k_BT}\nabla\Big(\mu_\beta - \tfrac{m_\beta}{m_S}\mu_S + z_\beta e_0\varphi\Big)\,, \qquad \text{for } \alpha\in\mathcal{I}\setminus\{S\}\,, \tag{2.6a}$$

$$\boldsymbol{\Sigma} = -p\mathbf{1} + \nu\operatorname{div}(\boldsymbol{v})\mathbf{1} + \eta(\nabla\boldsymbol{v} + \nabla\boldsymbol{v}^T) - \tfrac{1}{2}(1+\chi)\varepsilon_0|\nabla\varphi|^2\mathbf{1} + (1+\chi)\varepsilon_0\nabla\varphi\otimes\nabla\varphi\,. \tag{2.6b}$$

The phenomenological coefficients are diffusion coefficients $D_{\alpha\beta}$, bulk viscosity ν and shear viscosity η. The second law of thermodynamics requires $D_{\alpha\beta}$ positive definite, $\eta\geq 0$ and $\nu+\frac{2}{3}\eta\geq 0$. The driving force of the diffusion is the gradient of the (effective) electrochemical potential, which is given as

$$\mu_\alpha^{\mathrm{e}} = \mu_\alpha - \tfrac{m_\alpha}{m_S}\mu_S + z_\alpha e_0\varphi\,. \tag{2.7}$$

The derivation of suitable constitutive equations for liquid electrolytes can be found in [DGM13, DGL14, DGM18]. We refer to this material model as Dreyer-Guhlke-Landstorfer-Müller model (DGLM model).

The constraint (2.5) guarantees that the total mass density ρ is conserved, i.e.

$$\partial_t\rho + \operatorname{div}(\rho\boldsymbol{v}) = 0\,. \tag{2.8}$$

[1] The total stress tensor consists of the Cauchy and the Maxwell stress tensor. We refer to [DGM13, DGM18] for more details.

For constant mass density and vanishing viscosity, the momentum balance (2.4b) together with (2.6b) reduces to

$$\text{mechanical quasi-equilibrium:} \qquad \nabla p = -n^{\mathrm{F}} \nabla \varphi \, . \tag{2.9}$$

The term on the right hand side is the electrostatic approximation of the Lorentz force. In region with non-zero free charge density and an non-zero electric field, a pressure gradient results. In particular in the electrochemical double layer, where charge accumulates and the electric field is in the order of several volts per nm, large pressure are generated.

2.1 Continuum models for ion transport in electrolytes – a brief survey

In the literature various continuum models are applied to describe charge transport in electrolytes. In the context of nanopores the majority of electrolyte models are based on i) the classical Poisson–Nernst–Planck model (PNP-model) or ii) modified PNP models that we refer to as Bikerman model. Both types of models can be related to the general framework above and the DGLM model can be seen as a further extension step of these models.

Classical Nernst–Planck. The classical Nernst–Planck model, cf. [BF00, NTA04], is the most common electrolyte model for strongly diluted solutions, i.e. $n_\alpha \ll n_0$. The fluxes are chosen as

$$\boldsymbol{J}_\alpha = -D_{\alpha\alpha}\, m_\alpha \left(\nabla n_\alpha + n_\alpha \, \frac{z_\alpha e_0}{k_B T} \nabla \varphi \right) \qquad \text{for } \alpha = 1, \dots, N \, . \tag{2.10}$$

Here, a diagonal matrix of the diffusion coefficients is assumed, i.e. $D_{\alpha\beta} = 0$ for $\alpha \neq \beta$, that can be justified by a derivation of the more general Maxwell-Stefan model in the limit of strong dilution, see e.g. [BFS14]. From (2.10) we can reconstruct electrochemical potentials μ_α^{e} as

$$\mu_\alpha^{\mathrm{e}} = \widetilde{\mu}_\alpha^{ref} + k_B T \ln \frac{n_\alpha}{n} + z_\alpha e_0 \varphi \qquad \text{for } \alpha = 1, \dots, N \, , \tag{2.11}$$

where $\widetilde{\mu}_\alpha^{ref}$ is a reference potential, which in general depends on temperature. The total number density n is approximately equal to the number density n_S of the pure solvent and can be related to the specific volume of the solvent v_S^{ref},

$$n = n_S = \tfrac{1}{v_S^{ref}} \, . \tag{2.12}$$

In a liquid electrolyte, typically very thin charged boundary layers form, but in the bulk region, outside the boundary layers, the electrolyte is locally electroneutral, i.e. $n^{\mathrm{F}} = 0$. For vanishing velocity $\boldsymbol{v} \approx 0$, the electrolyte bulk can be described by the Nernst–Planck model consisting of (2.4b) and (2.10) together with $n^{\mathrm{F}} = 0$, see [DGM13, DGM15].

To describe also the charged boundary layers, the electroneutrality condition can be replaced by the Poisson equation (2.4a), leading to the PNP model. In the presence of non vanishing convection, the system can further be coupled to Navier-Stokes equations for the fluid flow (NS-PNP). In the strong dilution limit, the barycentric velocity $\boldsymbol{v}$ coincides with the solvent velocity and the total mass density is approximately given by the constant solvent mass density.

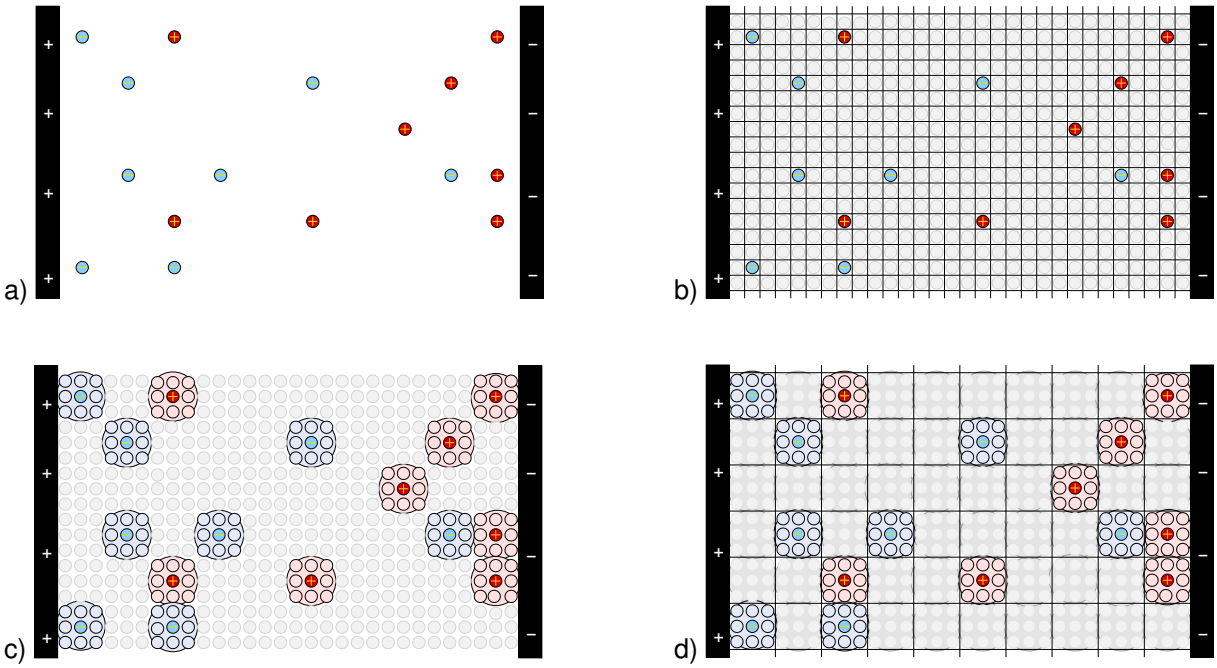

Figure 1: The same ion distribution, represented in different electrolyte models: a) in the Nernst–Planck model the solvent is not considered. b) Bikerman with lattice size given by the solvent molecule c) incompressible ideal mixture with solvated ion, d) Bikerman with lattice size given by the solvated ions.

Bikerman. Although the strong dilution assumption is often well justified in the bulk regions, in general it is not in the boundary layers. This leads to the well-known deficiency of the PNP model, the almost unbounded accumulation of ionic charge in the vicinity of a charge surface. Several authors proposed remedies where a common key feature of these extended Nernst–Planck models is the introduction of a finite length scale that is related to a molecular size and thereby defines an underlying lattice model for the electrolyte, cf. [Bik42, BAO97, KBA07, BSW12]. We refer to this kind of models as Bikerman model.

The Bikerman model employs a lattice model where the size of the cells in the lattice defines one specific volume v_S^{ref} for all of the species. One reasonable choice is to set v_S^{ref} such that for the pure solvent without any further constituents, the correct number density is attained, see Fig. 1b). The total number density is given by the lattice and thus it is constant

$$n = \frac{1}{v_S^{ref}} , \tag{2.13}$$

and also the maximal charge density has an upper bound. The effective electrochemical potentials are defined

$$\mu_\alpha^{\mathrm{e}} = \widetilde{\mu}_\alpha^{ref} + k_B T \ln \frac{n_\alpha}{n_S} + z_\alpha e_0 \varphi , \tag{2.14}$$

what is compatible with (2.7) if the specific volumes and the atomic masses of all species are equal, i.e.

$$m_\alpha = m_S , \qquad v_\alpha^{ref} = v_S^{ref} . \tag{2.15}$$

Moreover, the explicit dependency of μ_α^{e} on the solvent in (2.14) then can be removed by using (2.13) in the form $n_S = \frac{1}{v_S^{ref}} - \sum_{\alpha=1}^{N} n_\alpha$.

Incompressible ideal mixture of solvated ions (DGLM model). In the incompressible setting, the pressure p is an independent variable and the number densities have to satisfy the constraint

$$1 = \sum_{\alpha \in \mathcal{I}} \upsilon_\alpha^{ref} n_\alpha \,, \tag{2.16}$$

which defines an upper bound for the number densities. Here, the constants υ_α^{ref} denote the specific volume of constituent with index α. The chemical potentials μ_α are defined as

$$\mu_\alpha = \mu_\alpha^{ref} + \upsilon_\alpha^{ref} p + k_B T \ln(y_\alpha) \,, \tag{2.17}$$

where μ_α^{ref} is the reference potential, which depends in general on temperature. Thus, the (effective) electrochemical potentials are

$$\mu_\alpha^{\mathrm{e}} = \widetilde{\mu}_\alpha^{ref} + k_B T\big(\ln(y_\alpha) - \tfrac{m_\alpha}{m_S}\ln(y_S)\big) + (\upsilon_\alpha^{ref} - \tfrac{m_\alpha}{m_S}\upsilon_\alpha^{ref})p + z_\alpha e_0 \varphi \,, \tag{2.18}$$

where $\widetilde{\mu}_\alpha^{ref}$ collects the reference chemical potentials of ion and solvent.

Insertion of the chemical potential (2.17) into the mass fluxes (2.6a) yields the explicit expression for the fluxes

$$\boldsymbol{J}_\alpha = -\sum_{\beta=1}^{N} D_{\alpha\beta}\, m_\beta \Bigg(\nabla n_\beta + n_\beta \frac{z_\beta e_0}{k_B T}\nabla\varphi \tag{2.19}$$
$$+ \frac{n_\beta}{n_S}\Big[-\frac{m_\beta}{m_S}\nabla n_S - \frac{n_S}{n}\Big(1 - \frac{m_\beta}{m_S}\Big)\nabla n + \frac{n_S}{k_B T}\Big(\upsilon_\beta^{ref} - \frac{m_\beta}{m_S}\upsilon_S^{ref}\Big)\nabla p\Big]\Bigg).$$

Compared to the standard Nernst–Planck model, cf. (2.10), there are three additional terms highlighted here in blue. The first term represents the solvent-ion interaction, the second term takes into account the different size of the constituents and the third term represents the coupling of elastic effects and diffusion. All these terms vanish in the limit case of strong dilution, i.e. for $n_\alpha \ll n_S$. The Bikerman model contains the first of these three terms, For the second and the third term to vanish, it requires the assumption (2.15) of equal volume and equal mass for all species.

The incompressibility constraint (2.16) generalizes the lattice model of the Bikerman model by allowing the different species to have different specific volume. In polar solvents, i.e. in water, the charged ions build larger complexes with several of the solvent molecules. A solvated ion is said to consist of a center ion and the solvation shell. The solvent molecules in the solvation shell are not free to participate in the entropic mixing. Therefore, it is reasonable to consider the solvated ions as the constituents of the mixture and not the bare center ions without the solvation shell, cf. the illustration in Fig. 1c). As a consequence, the mixture consists of species with strongly different specific volume and mass. It is also possible, to use a common specific volume of the solvated ions to define a lattice of the Bikerman model. But this would imply that also the solvent is considered as consisting of larger compounds which are built from several solvent molecules without entropic interaction of the single solvent molecules, see Fig. 1d).

3 Nanopores

Specific assumptions. For the application to nanopores, in this paper we simplify the general model by the following assumptions:

- diagonal matrix of the diffusion coefficients, i.e. $D_{\alpha\beta} = 0$ for $\alpha \neq \beta$,
- no chemical reactions and no gravitation, i.e. $r_\alpha = 0$ and $\boldsymbol{b} = 0$.
- mechanical equilibrium, i.e. $\boldsymbol{v} \to 0$,
- mass-volume-ratio of all constituents is identical,

$$\frac{m_\alpha}{v_\alpha} = \frac{m_S}{v_S}\,, \qquad \text{for} \qquad \alpha = 1, \dots, N\,. \tag{3.1}$$

These assumptions yield i) the convective flow in the mass balances (2.5) can be ignored ii) the total mass density is constant and thus the total mass balance (2.8) is satisfied, iii) the mass fluxes (2.19) do not depend on pressure and iv) the momentum balance reduces to (2.9) and decouples from the partial mass balances. The remaining model equations are

$$\partial_t n_\alpha + \operatorname{div}(-\tfrac{D_{\alpha\alpha} n_\alpha}{k_B T} \nabla \mu_\alpha^{\mathrm{e}}) = 0, \qquad \text{for} \quad \alpha = 1, \dots, N \tag{3.2a}$$

$$-\operatorname{div}((1+\chi)\varepsilon_0 \nabla \varphi) = \sum_{\alpha=1}^{N} z_\alpha e_0 n_\alpha\,, \tag{3.2b}$$

$$v_S^{ref} n_S = 1 - \sum_{\alpha=1}^{N} v_\alpha^{ref} n_\alpha\,, \tag{3.2c}$$

with the (effective) electrochemical potentials

$$\mu_\alpha^{\mathrm{e}} = \widetilde{\mu}_\alpha^{ref} + z_\alpha e_0 \varphi + k_B T \times \begin{cases} \ln \frac{n_\alpha}{n_S^{ref}} & \text{Nernst–Planck}\,, \\ \ln \frac{n_\alpha}{n_S} & \text{Bikerman}\,, \\ \ln \frac{n_\alpha}{n} - \frac{v_\alpha^{ref}}{v_S^{ref}} \ln \frac{n_S}{n} & \text{DGLM}\,. \end{cases} \tag{3.3}$$

For the pore wall no adsorption of the electrolytic species and a fixed surface charge σ is assumed. We have the boundary conditions

$$-\tfrac{D_{\alpha\alpha} n_\alpha}{k_B T} \nabla \mu_\alpha^{e} \cdot \nu|_{\Omega_M} = 0\,, \tag{3.4}$$

$$\varepsilon_0 (1+\chi) \nabla \varphi \cdot \nu|_{\Omega_M} = \sigma\,. \tag{3.5}$$

2D approximation of a nanopore. We consider a 2D-cross-section of the pore which is symmetric with respect to the axis at $r = 0$. The coordinate in axial direction is denoted by x. The pore wall is described by a parameterization $R : (0, L) \to \mathbb{R}^+$ and it carries a surface charge σ that depends only on the axial variable x. The domain $\Omega \subset \mathbb{R}^2$ of the pore cross-section is given by

$$\Omega = \{(x, r) \mid 0 \leq x \leq L,\ |r| \leq R(x)\}\,. \tag{3.6}$$

At $x = 0$ and $x = L$ the pore domain is connected to the reservoirs on both sides of the membrane.

4 Asymptotics for large aspect ratio nanopores

4.1 Scaling

For the non-dimensionalization of the model equations we substitute the variables according to Tab. 1 and thereby we transform the computational domain to the unit square $(0, 1)^2$. We introduce two

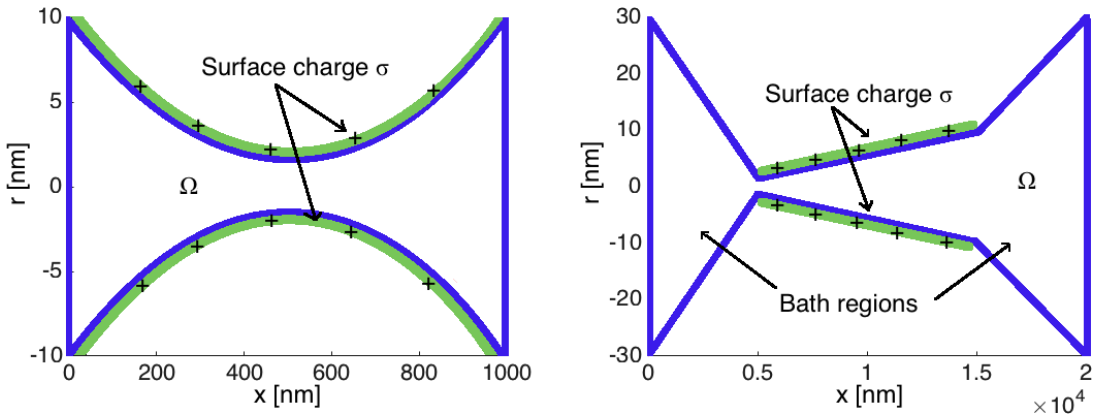

Figure 2: Sketches of the geometries considered for the nanopores.

Table 1: Substitution for the non-dimensionalization.

$x \to L^{ref}x$	$r \to R(x)R^{ref}r$	$t \to t^{ref}t$	$n_\alpha \to n^{ref}n_\alpha$	$\upsilon_\alpha^{ref} \to \frac{1}{n^{ref}}\upsilon_\alpha^{ref}$
$\varphi \to \frac{k_BT}{e_0}\varphi$	$\mu_\alpha \to k_BT\mu_\alpha$	$D_{\alpha\alpha} \to \frac{(L^{ref})^2}{t^{ref}}D_{\alpha\alpha}$	$\sigma \to \frac{(1+\chi)\varepsilon_0 k_BT}{e_0 R^{ref}}\sigma$	

dimensionless constants:

$$\widetilde{\lambda} := \sqrt{\frac{\varepsilon_0(1+\chi)k_BT}{e_0^2 n^{ref}(L^{ref})^2}}\,, \qquad \widetilde{\delta} := \frac{R^{ref}}{L^{ref}}\,. \tag{4.1}$$

The first constant is related to the Debye-length $\widetilde{\lambda}L^{ref}$, that characterize the wide of the electrical double layer at charged pore walls. The second constant is the aspect ratio of the pore. Both constants appear quadratic in the dimensionless system.

A nanopore filled with aqueous electrolyte is characterized by these scaling quantities

$$t^{ref} = 1\mathsf{s}\,, \qquad L^{ref} = 10^{-5}\mathsf{m}\,, \qquad R^{ref} = 10^{-9}\mathsf{m}\,, \tag{4.2}$$

$$n^{ref} = 1\mathsf{mol/L}\,, \qquad T = 300\mathsf{K}\,, \qquad \chi = 80\,. \tag{4.3}$$

These values imply for the dimensionless constants

$$\widetilde{\lambda}^2 \approx 10^{-8}\,, \qquad \widetilde{\delta}^2 \approx 10^{-8}\,, \tag{4.4}$$

For diffusion coefficients and the surface charges in the range of

$$D_{\alpha\alpha} = 10^{-9}\frac{\mathsf{m}^2}{\mathsf{s}}\,, \qquad \sigma = 10^{-1}\frac{\mathsf{C}}{\mathsf{m}^2}\,, \tag{4.5}$$

the corresponding dimensionless quantities are of order one. This motivates a second rescaling of the variables where now we introduce a small parameter $\varepsilon \approx 10^{-8}$ and the substitutions

$$\lambda^2 \to \varepsilon\widetilde{\lambda}^2\,, \qquad \delta^2 \to \varepsilon\widetilde{\delta}^2\,, \tag{4.6}$$

such that now λ^2 and δ^2 are of order one.

Summary of the dimensionless nanopore model. The nanopore model reads in dimensionless quantities

$$\partial_t n_\alpha - D_{\alpha\alpha}\big(\partial_x - \tfrac{R'}{R} r\partial_r\big)\big(n_\alpha \partial_x \mu_\alpha^e - n_\alpha \tfrac{R'}{R} r\partial_r \mu_\alpha^e\big) - \tfrac{1}{\varepsilon}\tfrac{D_{\alpha\alpha}}{\delta^2 R^2}\partial_r(n_\alpha \partial_r \mu_\alpha^e) = 0\,, \tag{4.7a}$$

$$-\lambda^2 \varepsilon(\partial_x - \tfrac{R'}{R} r\partial_r)(\partial_x \varphi - \tfrac{R'}{R} r\partial_r \varphi) + \tfrac{\lambda^2}{\delta^2 R^2}\partial_{rr}\varphi = \sum_{\alpha=1}^{N} z_\alpha n_\alpha\,, \tag{4.7b}$$

$$\upsilon_S^{ref} n_S = 1 - \sum_{\alpha=1}^{N} \upsilon_\alpha^{ref} n_\alpha\,. \tag{4.7c}$$

The dimensionless electrochemical potentials are define as

$$\mu_\alpha^{\mathrm{e}} = \widetilde{\mu}_\alpha^{ref} + z_\alpha \varphi + \begin{cases} \ln \frac{n_\alpha}{n_S^{ref}} & \text{Nernst–Planck}\,, \\ \ln \frac{n_\alpha}{n_S} & \text{Bikerman}\,, \\ \ln \frac{n_\alpha}{n} - \frac{\upsilon_\alpha^{ref}}{\upsilon_S^{ref}} \ln \frac{n_S}{n} & \text{DGLM}\,. \end{cases} \tag{4.8}$$

The dimensionless boundary conditions at the pore wall and the symmetry axis are

$$-D_{\alpha\alpha} n_\alpha \big(\partial_r \mu_\alpha^e - R' R \varepsilon \delta^2 (\partial_x - \tfrac{R'}{R}\partial_r)\mu_\alpha^e\big)|_{r=1} = 0\,, \qquad \partial_r n_\alpha|_{r=0} = 0\,, \tag{4.9a}$$

$$\tfrac{1}{\sqrt{\varepsilon\delta^2 (R')^2 + 1}}\big(\tfrac{1}{R}\partial_r \varphi - \delta^2 \varepsilon R'(\partial_x - \tfrac{R'}{R}\partial_r)\varphi\big)|_{r=1} = \sigma\,, \qquad \partial_r \varphi|_{r=0} = 0. \tag{4.9b}$$

4.2 Derivation of an asymptotic model

In this section we discuss a leading order problem in terms of ε that must be solved both in x and r direction. In order to find an asymptotic solution of system (4.7)-(4.9) in the limit $\varepsilon \to 0$, and with all other parameters of size $O(1)$, we assume the existence of expansions of the form

$$\varphi = \varphi^{(0)}(r,x,t) + \varepsilon\, \varphi^{(1)}(r,x,t) + \varepsilon^2\, \varphi^{(2)}(r,x,t) + \cdots\,, \tag{4.10a}$$

$$n_\alpha = n_\alpha^{(0)}(r,x,t) + \varepsilon\, n_\alpha^{(1)}(r,x,t) + \varepsilon^2\, n_\alpha^{(2)}(r,x,t) + \cdots\,, \tag{4.10b}$$

$$\mu_\alpha^{\mathrm{e}} = \mu_\alpha^{\mathrm{e},(0)}(r,x,t) + \varepsilon\, \mu_\alpha^{\mathrm{e},(1)}(r,x,t) + \varepsilon^2\, \mu_\alpha^{\mathrm{e},(2)}(r,x,t) + \cdots\,. \tag{4.10c}$$

These expansions are entered into the equations and boundary conditions. Then, the terms are sorted with respect to their polynomial order in ε. In the following we focus on the first order approximations of the equations and match the respective order in considered equations. For the simplicity of the presentation, we omit the superscripts $^{(0)}$, that are referring to the order in the expansion.

Leading order equations for the cross-sections. Introducing the expansions (4.10) into (4.7)-(4.9) provides us with the first order approximations of the the system which read

$$\partial_r \mu_\alpha^{\mathrm{e}} = 0\,, \qquad \text{for} \qquad \alpha = 1,\dots,N \tag{4.11a}$$

$$-\tfrac{\lambda^2}{\delta^2 R^2}\partial_{rr}\varphi = \sum_{\alpha=1}^{N} z_\alpha n_\alpha\,, \tag{4.11b}$$

$$\upsilon_S^{ref} n_S = 1 - \sum_{\alpha=1}^{N} \upsilon_\alpha^{ref} n_\alpha\,. \tag{4.11c}$$

The boundary conditions simplify to

$$\partial_r \mu_\alpha^e|_{r=1} = 0\,, \qquad \partial_r n_\alpha|_{r=0} = 0\,, \tag{4.12a}$$

$$\partial_r \varphi|_{r=1} = R\sigma\,, \qquad \partial_r \varphi|_{r=0} = 0\,. \tag{4.12b}$$

Leading order equations for the averaged ion concentrations. In the following, we indicate quantities that are averaged over the r-coordinate by a superscript bar, i.e. for a generic function u the corresponding averaged quantity is $\bar{u} = \int_0^1 u\, dr$. The integration of the system (4.7) in r-direction leads to the leading order system for the averaged number densities,

$$\partial_t \bar{n}_\alpha - \tfrac{D_{\alpha\alpha}}{R}\partial_x(R\,\bar{n}_\alpha\,\partial_x \bar{\mu}_\alpha^{\mathrm{e}}) = 0\,, \qquad \alpha = 1,\dots,N\,, \tag{4.13a}$$

$$-\tfrac{\lambda^2}{\delta^2 R}\sigma = \sum_{\alpha=1}^{N} z_\alpha \bar{n}_\alpha\,, \tag{4.13b}$$

$$v_S^{ref}\bar{n}_S = 1 - \sum_{\alpha=1}^{N} v_\alpha^{ref}\bar{n}_\alpha\,. \tag{4.13c}$$

For the derivation we used the boundary conditions (4.9) and the leading order equations for the cross-section (4.11).

4.3 Reduction to averaged 1D problem

The asymptotic analysis above decouples the fluxes in x and in r direction and thereby splits the full 2D system into two coupled 1D systems. The equation system (4.13a)–(4.13c) determines the evolution of the averaged number densities along the nanopore and the equation system (4.11a)–(4.11c) determines the specific ion concentration profiles in each cross-section of the nanopore. A similar coupled 1+1D system for the rotational symmetric case is the basis for the quasi-1D PNP model developed in [MPWR18]. In the following we derive a reduction from the asymptotic 1+1D system to a single 1D system, that is also applicable for the Bikerman and in the DGLM model.

Exact solution in the cross-section. At first we integrate the inner equations (4.11a) for $\alpha = 1,\dots,N$, as well as for $\alpha = S$, to get implicit representations of the mole fractions, that reads

$$y_\alpha = y_\alpha^0\,\exp(-z_\alpha(\varphi-\varphi^0)) \times \begin{cases} 1 & \text{Nernst–Planck}\,, \\ \frac{y_S}{y_S^0} & \text{Bikerman}\,, \\ \left(\frac{y_S}{y_S^0}\right)^{v_\alpha^{ref}/v_S^{ref}} & \text{DGLM}\,. \end{cases} \tag{4.14}$$

Here the y_α^0 and φ^0 denotes mole fractions and potentials at $r = 0$ respectively. The mole fraction of the solvent is determined by $(2.3)_{\text{right}}$,

$$y_S = 1 - \sum_{\alpha=1,\dots,N} y_\alpha\,, \tag{4.15}$$

and the total number density n can be then determined using the equation (4.11c).

Form the equations (4.14) and (4.11c) we conclude that the number densities n_α can be expressed as functions of the electric potential φ and the number densities n_α^0 and electric potential φ^0.

Multiplication of the Poisson equation (4.13b) by $\partial_r\varphi$ yields

$$-\tfrac{\lambda^2}{2\delta^2 R^2}\partial_r(\partial_r\varphi)^2 = \Big(\sum_{\alpha=1}^{N} z_\alpha n_\alpha\Big)\partial_r\varphi\,. \tag{4.16}$$

In the Nernst–Planck case, the right hand side of (4.16) can be expressed as the r derivative of a function that depends on $\varphi-\varphi^0$ and n_α^0. For Bikerman and DGLM, we differentiate (4.15) with respect to r and by use of (4.14) and (4.11c) we get the identity

$$\tfrac{1}{\upsilon_S^{ref}}\partial_r \ln(y_S) = \Big(\sum_{\alpha=1}^{N} z_\alpha n_\alpha\Big)\partial_r\varphi\,. \tag{4.17}$$

We use the identity to replace the free charge density in the Poisson equation (4.11b) by the r- derivative of $\ln(y_S)$. This allows us to integrate the Poisson equation to obtain a relation between the r- derivative of the electric potential and the mole fraction of the solvent.

$$\partial_r\varphi = \operatorname{sgn}(\sigma) R\tfrac{\sqrt{2}\delta}{\lambda}\sqrt{P(\varphi-\varphi^0, n_1^0,\dots,n_N^0)}\,, \tag{4.18}$$

where P is defined as [2]

$$P(\varphi-\varphi^0, n_1^0,\dots,n_N^0) = \begin{cases} \sum_{\alpha=1}^{N} n_\alpha^0\big(\exp(-z_\alpha(\varphi-\varphi^0))-1\big) & \text{Nernst–Planck}\,,\\ \frac{1}{\upsilon_S^{ref}}\ln\big(\frac{n_S^0}{n_S}\big) & \text{Bikerman}\,,\\ \frac{1}{\upsilon_S^{ref}}\ln\big(\frac{y_S^0}{y_S}\big) & \text{DGLM}\,. \end{cases} \tag{4.19}$$

Let φ^R denote the electric potential at the pore wall. The relation (4.18) and the boundary conditions (4.12b) relate the potential difference $\varphi^R-\varphi^0$ to the surface charge and number densities at $r=0$,

$$\sigma = \operatorname{sgn}(\sigma)\tfrac{\sqrt{2}\delta}{\lambda}\sqrt{P(\varphi^R-\varphi^0, n_1^0,\dots,n_N^0)}\,. \tag{4.20}$$

The number densities for $\alpha=1,\dots,N$, as well as for $\alpha=S$ can now be expressed in terms of P as

$$n_\alpha = n_\alpha^0\exp(-z_\alpha(\varphi-\varphi^0))\times\begin{cases} 1 & \text{Nernst–Planck}\,,\\ \exp(-\upsilon_\alpha^{ref}P) & \text{Bikerman}\,,\\ \dfrac{n}{n^0}\exp(-\upsilon_\alpha^{ref}P) & \text{DGLM}\,. \end{cases} \tag{4.21}$$

When evaluating the mean values of the number densities, we use this relation to substitute the integration with respect to r by an integration with respect to φ for the averaging. To compensate a singularity in the integral, we average the deviation from the values at the axis, i.e. $\bar n_\alpha = n^0 + \overline{n_\alpha - n^0}$, and get

$$\bar n_\alpha = n_\alpha^0 + \tfrac{1}{R}\tfrac{\lambda}{\sqrt{2}\delta}\int_0^{\varphi^R-\varphi^0}\frac{n_\alpha-n_\alpha^0}{\sqrt{P(\widetilde\varphi, n_1^0,\dots,n_N^0)}}\,d\widetilde\varphi \qquad \alpha=1,\dots,N\,. \tag{4.22}$$

As the first order electrochemical potentials are r independent (see equation (4.11a)), the mean chemical potentials for $\alpha=1,\dots,N$ are given by their respective values at $r=0$,

$$\bar\mu_\alpha^e = \widetilde\mu_\alpha^{ref} + z_\alpha\varphi^0 + \begin{cases} \ln\frac{n_\alpha^0}{n_S^{ref}} & \text{Nernst–Planck}\,,\\ \ln\frac{n_\alpha^0}{n_S^0} & \text{Bikerman}\,,\\ \ln\frac{n_\alpha^0}{n^0} - \frac{\upsilon_\alpha^{ref}}{\upsilon_S^{ref}}\ln\frac{n_S^0}{n^0} & \text{DGLM}\,. \end{cases} \tag{4.23}$$

[2] This P is in fact related to the pressure, or more precisely it is the pressure difference $p-p^0$, and (4.17) is a variant of the momentum balance (2.9). Readers who feel uncomfortable with the introduction of a pressure in the context of Nernst–Planck or Bikerman models can treat it as just a shorthand notation for the corresponding expression in (4.19).

Resulting 1D system and 2D reconstruction. The variables φ^0 and n^0_α for $\alpha = 1, \dots, N$, as well as φ^R and $\bar{n}^0_\alpha$ for $\alpha = 1, \dots, N$ are determined by a system consisting of one dimensional PDEs in x-direction (4.13a) and (4.13b), and in addition for each point in x the non-linear algebraic equations (4.20) and (4.22). The system reads

$$\partial_t \bar{n}_\alpha = \tfrac{D_{\alpha\alpha}}{R} \partial_x (R\, \bar{n}_\alpha\, \partial_x \bar{\mu}^{\mathrm{e}}_\alpha) \qquad \alpha = 1, \dots, N\,, \tag{4.24a}$$

$$-\tfrac{\lambda^2}{\delta^2 R} \sigma = \sum_{\alpha=1}^{N} z_\alpha \bar{n}_\alpha\,, \tag{4.24b}$$

$$\sigma = \operatorname{sgn}(\sigma) \tfrac{\sqrt{2}\delta}{\lambda} \sqrt{P(\varphi^R - \varphi^0, n^0_1, \dots, n^0_N)}\,. \tag{4.24c}$$

$$\bar{n}_\alpha = n^0_\alpha + \tfrac{1}{R} \tfrac{\lambda}{\sqrt{2}\delta} \int_0^{\varphi^R - \varphi^0} \frac{n_\alpha - n^0_\alpha}{\sqrt{P(\widetilde{\varphi}, n^0_1, \dots, n^0_N)}}\, d\widetilde{\varphi} \qquad \alpha = 1, \dots, N\,, \tag{4.24d}$$

For the averaged potentials $\bar{\mu}^{\mathrm{e}}_\alpha$ (4.23) is applied. To get n^0_S, (4.11c) is used,

$$\upsilon^{ref}_S n^0_S = 1 - \sum_{\alpha=1}^{N} \upsilon^{ref}_\alpha n^0_\alpha\,. \tag{4.25}$$

In the Nernst–Planck case the function P is explicitly determined by (4.19) as a function of n^0_α and φ^0. In contrast for the Bikerman and DGML model P is implicitly determined by equation

$$n_S + \sum_{\alpha=1}^{N} n_\alpha = n\,, \tag{4.26}$$

together with the representation (4.21) of the number densities.

Finally, a 2D solution can be recovered in a post processing step. Given the solution φ^0, φ^R and n^0_α, we use (4.11b) to determine φ in all of Ω, i.e.

$$-\tfrac{\lambda^2}{\delta^2 R^2} \partial_{rr} \varphi = \sum_{\alpha=1}^{N} z_\alpha n_\alpha(\varphi, P)\,, \tag{4.27a}$$

$$\varphi|_{r=0} = \varphi^0\,, \qquad \varphi|_{r=R} = \varphi^R\,, \tag{4.27b}$$

$$n(\varphi, P) = \sum_{\alpha=1}^{N} n_\alpha(\varphi, P) + n_S(\varphi, P)\,, \tag{4.27c}$$

$$1 = \sum_{\alpha=1}^{N} \upsilon^{ref}_\alpha n_\alpha(\varphi, P) + \upsilon^{ref}_S n_S(\varphi, P)\,, \tag{4.27d}$$

where we again use the representation (4.21) for n_α.

5 Numerical study

In this section we present numerical study focused on two questions:

- How accurate is the 1D-method derived in the Section 4.3 in comparison with the solution of the 2D model?

- What is the influence of the different solvation models as discussed in previous sections?

To answer these questions we study two, experimentally driven, pore examples: (i) a trumpet shaped pore and (ii) a conical pore geometry which are shown in Fig. 2. We consider a binary electrolyte consisting only of the solvent and – for simplicity – monovalent anions and cations and use the indices $\alpha \in \{A, C\}$ instead of $\alpha \in \{1, 2\}$ for referencing the ionic species. Further we assume that the number of solvent molecules in the solvation shell of the ions is equal. We refer to the solvation shell number as κ. The atomic masses and the specific volume of the ions are given by the simple relation

$$m_\alpha = (1+\kappa) m_S \,, \qquad\qquad \upsilon_\alpha^{ref} = (1+\kappa)\upsilon_S^{ref} \qquad \alpha = A, C \,. \tag{5.1}$$

By this assumption the mass-volume-ratio of all constituents is equal and the constraint (3.1) is satisfied.

5.1 Comparison 1D and 2D model

In this section we compare the 1D and 2D solutions for the DGLM model with $\kappa = 0$ and with $\kappa = 10$. The case $\kappa = 0$ coincides with the Bikerman model where the lattice size is given by the number density of the pure solvent. We also compared the 1D and 2D results from the Nernst–Planck model and found only minor differences compared to the Bikerman ($\kappa = 0$) case. Therefore we omit these results here.

The computations are performed with the parameters given in Table 2. On the left and the right domain boundary the surface charge vanishes and the electric potential and the number densities are thus constant in r direction. The prescribed potential difference between the left and the right boundary is denoted by V_{LR} and the number densities on the left and right boundary are set to the values n_{AC}^{bath} that correspond to the bulk concentrations in the baths on both sides of the pore.

Table 2: Parameters used in the numerical computations.

$k_B \approx 1.3806488 \times 10^{-23}\,\mathrm{J/K}$	$T = 300\,\mathrm{K}$	
$e_0 \approx 1.602176565 \times 10^{-19}\mathrm{C}$	$\varepsilon_0 \approx 8.85418781762^{-12}\mathrm{C/(V\,m)}$	$\sigma_0 = 1\,e_0/\mathrm{nm}^2$
$\chi = 77.5$	$z_A = -1$	$z_C = +1$
$(\upsilon_S^{ref})^{-1} = 55\,\mathrm{mol/L}$	$V_{LR} = 0.2\,\mathrm{V}$	$n_{A/C}^{\text{bath}} = 0.1\,\mathrm{mol/L}$

Numerical methods For the 1D problem, we use a P1 finite element method for the stationary version of (4.24a), i.e. we discretize

$$\int_0^L \partial_x \xi \cdot R\,\bar{n}_\alpha\,\partial_x \bar{\mu}_\alpha \,\mathrm{d}x = 0 \qquad \text{for all testfunctions } \xi \,, \tag{5.2}$$

where we apply element wise constant approximation of $R\,\bar{n}_\alpha$ by its value in the element mid point. For simplicity, a uniform mesh in x-direction is used and the integral in (4.22) is approximated by trapezoidal rule with a uniform partition and 500 evaluation points. The resulting non-linear system is solved by Newton's method and implemented for use with GNU Octave and MATLAB.

To solve the full 2D steady state system, i.e. equations (2.11), we used two different implementations.

On the one hand, a variant of the method described in in [MPWR18] applying a standard P1 finite element discretisation and a Gummel iteration, [Gum64] is used to solve the problems for the Bikerman

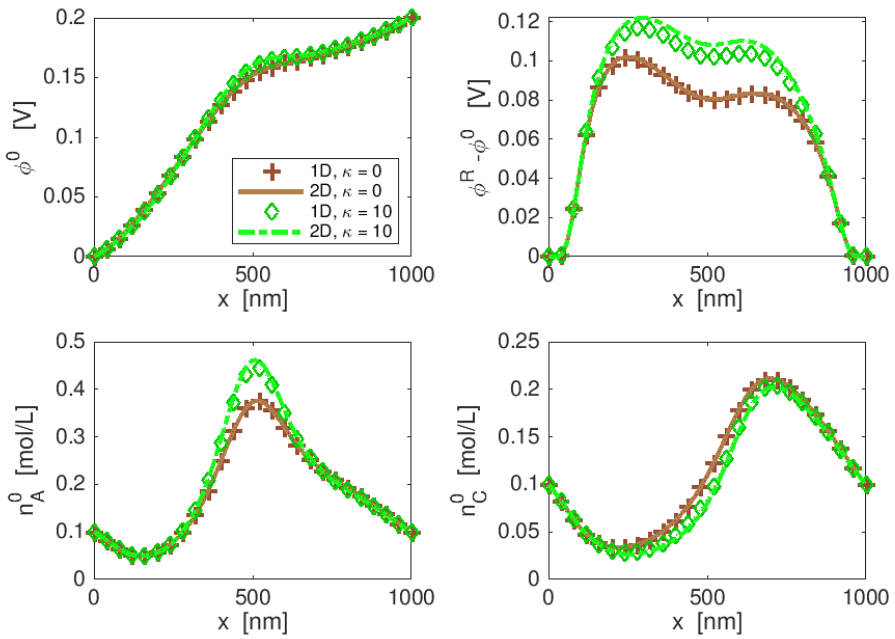

Figure 3: Comparison of the 1D and 2D solution for the trumpet shape pore. We observe good agreement between the 1D and 2D solution along the line $r = 0$ (functions $\varphi^0(x)$, $n_A^0(x)$ and $n_C^0(x)$). In addition, $\varphi^0(x) - \varphi^R(x)$ is displayed in the upper right figure to show the agreement between the 1D and the 2D computations on the pore walls.

model ($\kappa = 0$). We use non-uniform meshes that are strongly refined at the charged pore walls in order to properly resolve the Debye layers. The meshes are created using Netgen [Sch97], while we use MATLAB to assemble and solve the corresponding discrete systems. Because of the different length scales and the boundary layer scale we use a highly anisotropic mesh of 7×10^5 triangular elements.

On the other hand the method described in [Fuh15, Fuh16] is used to solve the problems for the DGLM model ($\kappa = 10$). It is based on a re-formulation of the system in terms of (effective) species activities $a_\alpha = \exp\left(\frac{\mu_\alpha - \frac{m_\alpha}{m_S}\mu_S}{k_B T}\right)$ and a two point flux finite volume method based on a thermodynamically consistent modification of the Scharfetter–Gummel flux [SG69]. Here, the resulting non-linear systems are solved via Newton iteration and parameter embedding. The discretization meshes are created from an anisotropic rectangular mesh with graded refinement in the vicinity of the pore wall and subsequent transformation to the pore geometries. The method is implemented within the C++/python based framework pdelib [JF+18].

Solutions from both codes where tested for coincidence for the classical Nernst–Planck and the Bikerman model.

Trumpet shape geometry. We consider a trumpet shaped pore like in Fig. 2. The length of the pore is $L^{ref} = 1000$nm and a radius is varying form 1.5nm to 10nm . This pore shape is usually obtained by the double etching technique and due to its symmetry in the x direction shows different behavior then the more popular conical shaped pore. The pore boundary is given by

$$\frac{R(x)}{R^{ref}} = \left(34\left(\tfrac{x}{L^{ref}}\right)^2 - 34\tfrac{x}{L^{ref}} + 10\right), \tag{5.3}$$

where we chose $R^{ref} = 1$nm. We assume a smooth charge distribution of the form

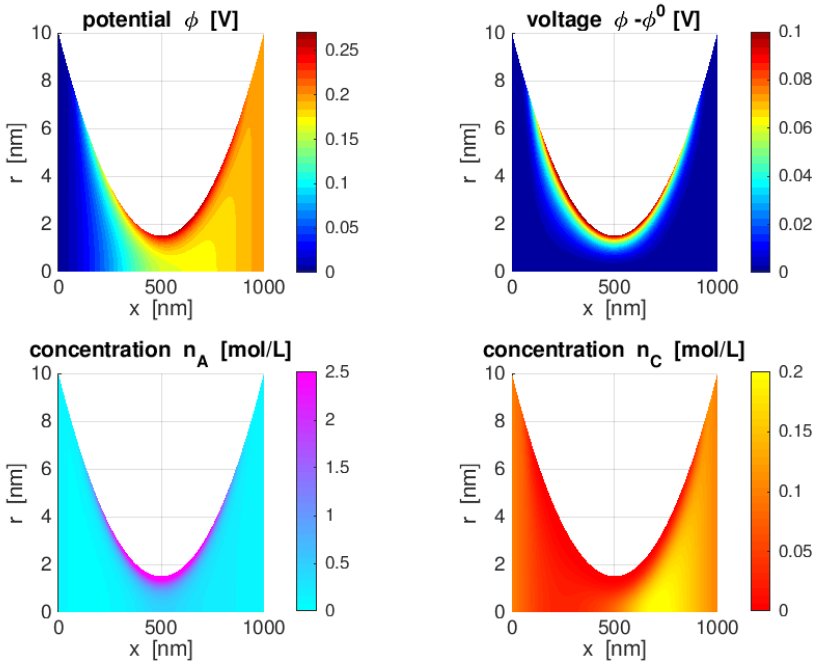

Figure 4: Reconstructed 2D solution based on the 1D solution with $\kappa = 10$ from Fig. 3. Only the upper half of the symmetric solution is displayed.

$$\sigma(x) = \sigma_0 \exp\left(1 + \frac{(L^{ref})^2}{(2x - L^{ref})^2 - (L^{ref})^2}\right). \tag{5.4}$$

The solution of the 1D problem is shown in Fig. 3. We observe that on the center line $r = 0$ in x direction the electric potential is not linear but instead but shows a stronger growth on the left side of the pore center at $x = 500$nm and a slower growth to the right of the center. The anions show some accumulation in the middle of the pore where the positive surface charge is the highest. The diffusion of cations from the right to the left side is hindered by the pore resulting in accumulation "before" and depletion "behind" the pore. Fig. 4 shows a 2D reconstruction for $\kappa = 10$. We observe a very sharp layer near the charged pore wall where the anions accumulate to compensate the surface charge.

Comparing the solution obtained with the 1D model with the results of the full 2D computations show very good agreement along the center line $r = 0$ and for the potential difference between the pore wall and the center line, cf. Fig. 3. A more detailed comparison of the 1D and 2D results and of the impact of the model parameter κ, can be obtained from cross-sections of the (reconstructed 2D) solutions for fixed values of the variable x. In Fig. 5, cross-sections are displayed in the pore middle at $x = 500$nm and at some distance to the left and right. Again, we observe perfect agreement between the 1D and 2D solutions over the complete distance of the cross-sections. The potential shows in all cases similar profiles from $r = 0$ to $r = R(x)R^{ref}$ with an increase in the order of 0.08V. At $x = 500$nm we see that, due to the higher concentration at $r = 0$, the anions accumulate very strongly in front of the charged pore wall, reaching a concentration of 7mol/L for $\kappa = 0$. For $\kappa = 10$ the anion concentration is significant lower at $n_A \approx 3.5$mol/L what is still considerably lower than the saturation limit of 5mol/L for this case. The cations are repelled from the positively charged wall, leading to similar profiles with respect to r, only starting from a significantly higher level for $x = 800$nm.

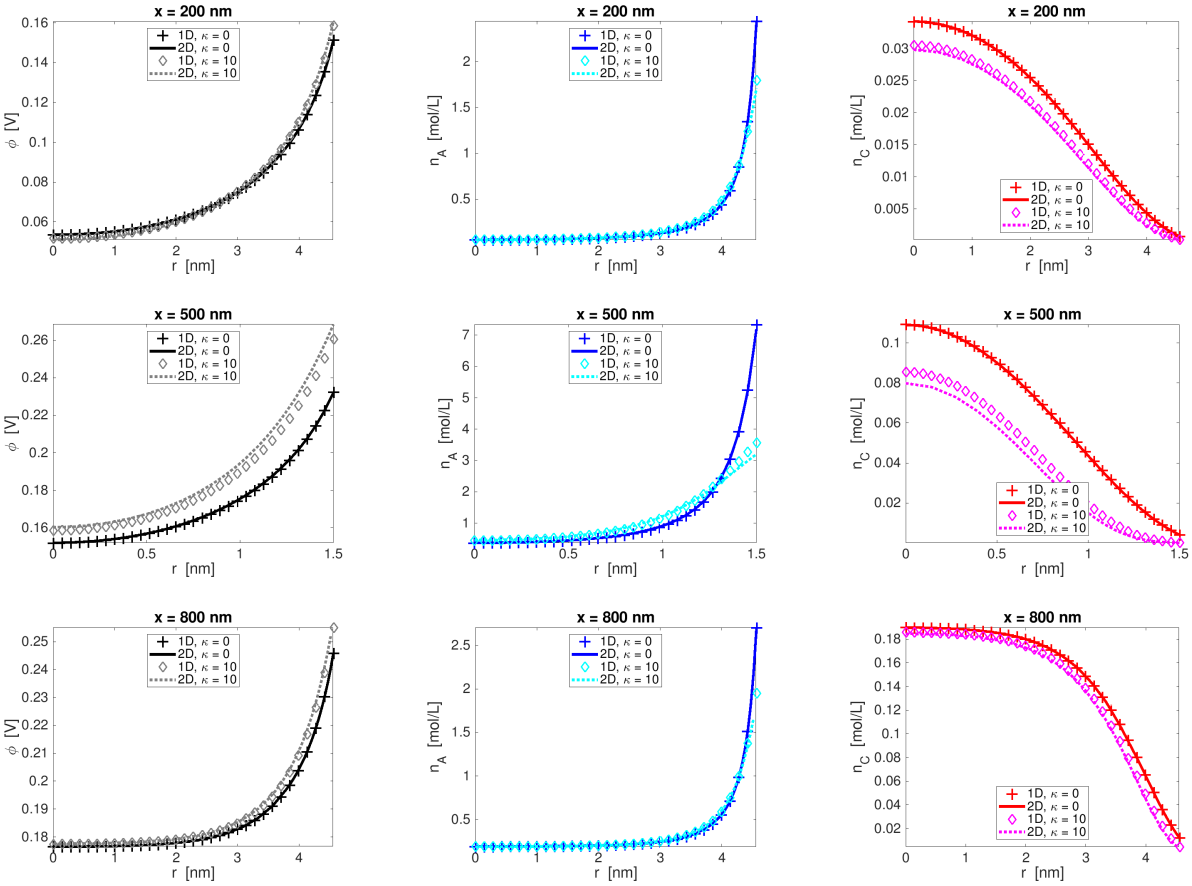

Figure 5: Cross sections of the potential and the number densities at $x = 200$nm (top row), $x = 500$nm (middle row) $x = 800$nm (bottom).

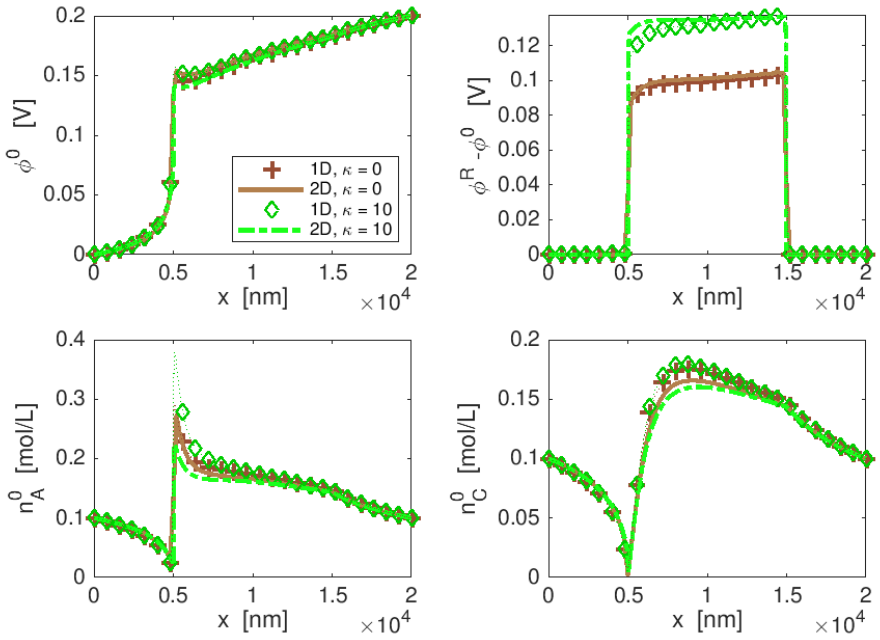

Figure 6: Comparison of the 1D and 2D solution for the conical shape pore. The computed 1D solution $\varphi^0(x)$, $n_A^0(x)$ and $n_C^0(x)$ agree with the corresponding 2D solution. In addition, $\varphi^0(x) - \varphi^R(x)$ is displayed in the upper right figure and also shows agreement between the 1D and the 2D computations.

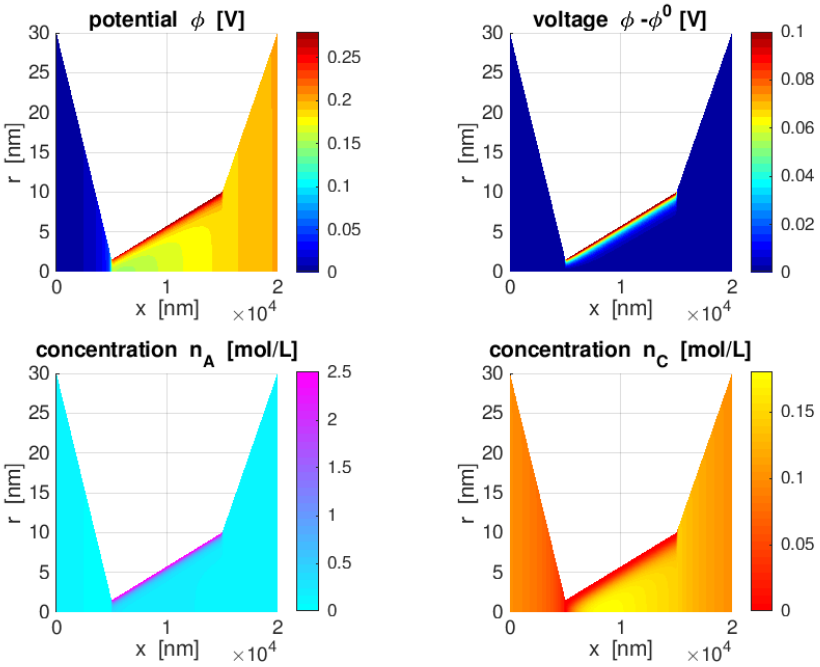

Figure 7: Reconstructed 2D solution based on the 1D solution with $\kappa = 10$ from Fig. 6. Only the upper half of the symmetric solution is displayed.

Conical shape geometry. Motivated by experimental work on pores with conical shape obtained using the etching technique, we consider a conically shaped pore of length $L^{ref} = 10000$nm with radius varying between 1.5nm and 10nm which corresponds with the polyethylene terephthalate (PET) nanopore, as used by Siwy [SAB+03]. It is well known that such narrow tips strongly influences the ion transport through the pore [PWB+13]. We include two bath regions of 5000nm length each. The computational domain is thus described by

$$\frac{R(x)}{R^{ref}} = \begin{cases} -28\left(\frac{2x-L^{ref}}{L^{ref}}\right) + 2 & \text{for } 0 \le \frac{x}{L^{ref}} \le \frac{1}{2}\,, \\ 8\left(\frac{2x-L^{ref}}{2L^{ref}}\right) + 2 & \text{for } \frac{1}{2} \le \frac{x}{L^{ref}} \le \frac{3}{2}\,, \\ 20\left(\frac{2x-3L^{ref}}{L^{ref}}\right) + 10 & \text{for } \frac{3}{2} \le \frac{x}{L^{ref}} \le 2\,. \end{cases} \tag{5.5}$$

We consider a pore with surface charge density inside the pore which corresponds with $5000\text{nm} < x < 15000\text{nm}$ and zero outside this section.

$$\sigma(x) = \sigma_0 \left(\tfrac{1}{2} + \tfrac{1}{2}\tanh\left(300\tfrac{2x-L^{ref}}{2L^{ref}}\right)\right)\left(\tfrac{1}{2} + \tfrac{1}{2}\tanh\left(-300\tfrac{2x-3L^{ref}}{2L^{ref}}\right)\right). \tag{5.6}$$

The solution of the 1D problem is shown in Fig. 6. We observe a very sharp, step-like transition layer of the electric potential at the narrow opening of the pore at $x = 5000$nm. The potential difference between the pore wall and the center line approaches a plateau inside the pore. The ion concentrations also show the sharp layers at $x = 5000$nm with accumulation on the right side of the narrow opening and depletion to the left. The anions show a sharp peak of the concentration directly right to the narrow opening. Fig. 7 shows a 2D reconstruction of the 1D solution for $\kappa = 10$. As in the parabolic case, we observe a very sharp layer near the charged pore wall.

The solutions from the 1D model show to a large extend good agreement with the results from the full 2D computations along the center line $r = 0$, cf. Fig. 6. While the potential difference between the pore wall and the center line agrees very well between the 1D and the 2D results, there is some deviation

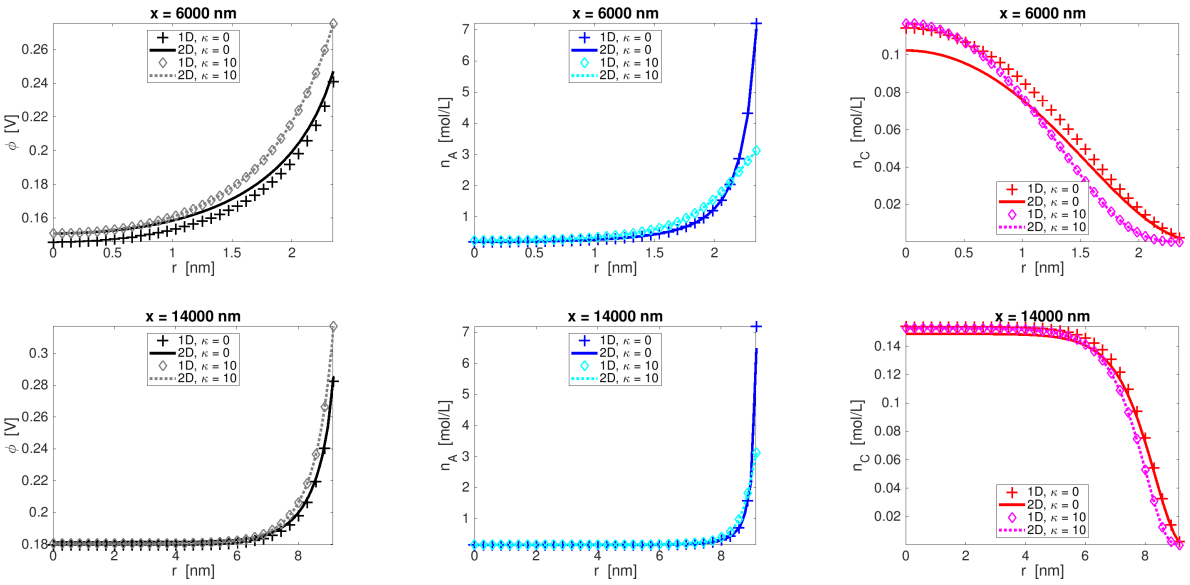

Figure 8: Cross sections of the potential and the number densities at $x = 6000$nm (top row), $x = 14000$nm (bottom) for the conical pore.

between the values on the center line near the narrow opening of the pore. In particular when looking at $\kappa = 10$, we observe that the peak in n_A^0 is more pronounced in the 1D simulations compared to the corresponding full 2D case. This indicates limitations of the asymptotic model in situations where sharp peaks in x direction occur. Cross-sections of the (reconstructed 2D) solutions for fixed x are shown in Fig. 8. At $x = 600$nm we again observe the very strong accumulation of anions in front of the charged pore wall, reaching a concentration of $7\text{mol}/\text{L}$ for $\kappa = 0$ and $n_A \approx 3.5\text{mol}/\text{L}$ for $\kappa = 10$.

Both examples – trumpet shape and conical pore – have also been solved numerically for the Poisson–Nernst–Planck model. As good agreement between the results from the 1D model and the 2D model was observed and the PNP model has the simplest structure among the models discussed here we do not present obtained results.

5.2 Solvation effect study for PNP, Bikerman and DGLM model

The Nernst–Planck model is build on the dilute solution assumption, and therefore is lacking any mechanism for volume exclusion. In the Bikerman model the size exclusion mechanism is introduced but as in the considered test cases the anion accumulation reaches only $7\text{mol}/\text{L}$, whereas the saturation limit in this case is the mole density of the pure solvent ($55\text{mol}/\text{L}$), the volume exclusion still has no significant impact on the ion concentration. To reach higher anion concentration and and observe the exclusion effects in the Bikerman model ($\kappa = 0$), it would be necessary to increase the surface charge significantly (although the chosen value of $1e_0/\text{nm}^2$ is already high) or consider higher concentrations in the bath regions.

In the profiles of n_A in Fig. 5 and Fig. 8, we observe that the larger specific volume $v_{A/C}^{ref}$ for $\kappa = 10$ effectively reduces the ion concentration already before getting close to the saturation limit of $5\text{mol}/\text{L}$ in this case. Thus it is reasonable to choose the lattice size in the Bikerman model according to the volume of the solvated ions as $(1 + \kappa)v_S^{ref}$ and then to compare the results with the DGLM model with the same solvation number.

In the following, we compare only the results of the 1D computations, which already have shown to be

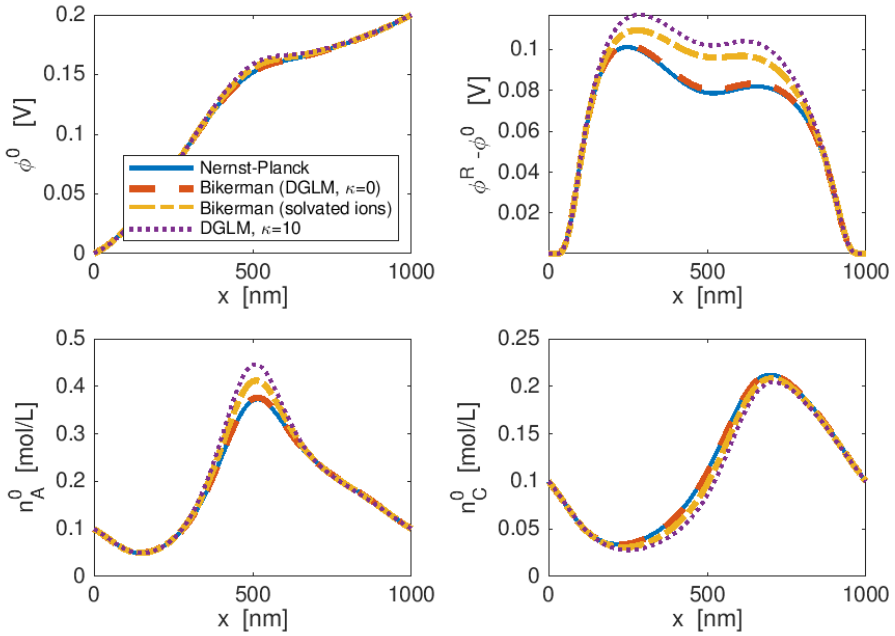

Figure 9: Comparison of different electrolyte models for the parabolic shape pore. Solvation effect leads to higher potential differences $\varphi^R - \varphi^0$ between the center line and the wall and stronger anion accumulation on the center line at the narrowest part of the pore.

in good agreement with the 2D solutions. The computations in this section were again performed using the parameters listed in Table 2.

Trumpet shape geometry. For all of the four considered models, the potential φ^0 along the center line at $r = 0$ is very similar, see Fig. 9. The largest differences can be observed in the region where the pore is the narrowest. Much more pronounced are the differences between the models for $\varphi^R - \varphi^0$. Here, the models containing solvation effects show a considerably higher potential difference than the Nernst–Planck and the Bikerman model without solvation. Moreover, the different treatment of the solvent causes a larger voltage $\varphi^R - \varphi^0$ in the DGLM model compared to the Bikerman model with solvated ions. The anion concentration n_a^0 along the center line shows a peak at the narrowest part of the pore where the charged pore wall with its adjacent diffuse charge layer gets closest to the center line. The peak height is almost the same for Nernst–Planck and Bikerman with $\kappa = 0$, but is larger for Bikerman with $\kappa = 10$ and is highest for the DGLM model. This higher anion concentration n_A^0 for $\kappa = 10$ is a consequence of the limitation of the space charge due to incompressibility and the large specific volume of the solvated ions which requires a larger boundary layer width to compensate the surface charge of the wall. The Bikerman model without solvated ions gives similar results to the Nernst–Planck as the summarized ion concentration is much smaller then the saturation level at $55\text{mol}/\text{L}$.

Conical shape geometry. For the conical pore, a comparison of the different electrolyte model, see Fig. 10, leads to the same conclusions as for the trumped shaped pore above.

The value $\phi^R - \phi^0$ is essentially the zeta potential [Hun13]. As observed above, the introduction of the solvation effect increases the zeta potential. In the absence of the mechanical equilibrium assumption taken for this contribution, according to the Helmholtz-Smoluchowski theory for pores with

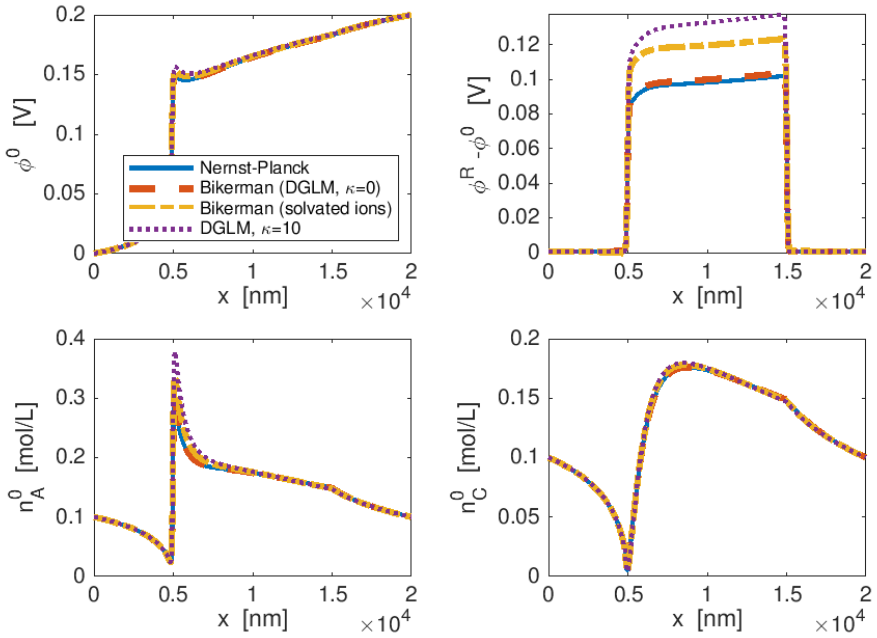

Figure 10: Comparison of different electrolyte models for the conical shape pore. Solvation effect leads to higher potential differences $\varphi^R - \varphi^0$ between the center line and the wall and stronger anion accumulation on the center line at the narrowest part of the pore.

non-overlapping Debye layers this would lead to a proportionally increased electroosmotic velocity, see also [FGL$^+$18] for discussion.

6 Conclusions and discussion

The asymptotic analysis used in this paper leads to quasi-equilibrium conditions governing the system in the cross sections perpendicular to the pore axes. This allows the effective dimension reduction of the model to a one dimensional situation by the use of implicit representations that are known for equilibrium solutions. This procedure can be applied for a variety of material models for the electrolyte: to the classical PNP model, but also – for the first time – to models containing volume exclusion effects like the Bikerman model and to models that in addition take solvation effects into account.

The numerical study demonstrates that the asymptotic 1D models can approximate the results of the full 2D models very closely, but at a considerably lower computational cost. In steady state, the profile of the electric potential and the ion distribution can be accurately reproduced by the dimension reduced asymptotic models. We observe differences between the different electrolyte models. In general, volume exclusion effects limit the charge accumulation in front of the charged wall. Nevertheless, going from the PNP model to the Bikerman model where the particle volume is given by the number density of the pure solvent, i.e. $55\text{mol}/\text{L}$, we observe almost no difference in the counter ion accumulation in front of the charged wall. This result might seem surprising at the first sight, and it seems to suggests that the simpler PNP model without volume exclusion effects might be preferable over more complex models like Bikerman or DGLM. But, one has to notice that the maximal archived number density is only about $7\text{mol}/\text{L}$ and thus too low for the volume exclusion mechanism to get relevant. Given realistic values of the surface charge, in the range of $1e_0/\text{nm}^2$ that we used here, therefore sufficiently large

complexes like solvated ions are need in order for the volume exclusion to have a visible effect. Then, the resulting ion distribution shows considerably less steep concentration gradients but also results in higher potential differences (ζ potential) between the pore wall and the center line of the pore. In further extended models, which take electro-osmotic flow into account, cf. [FGL$^+$18], this wider spreading of charge in the boundary layers can be expected to cause an increase of the flow velocity and thereby might contribute to the total current flow though the pore.

In the example of the conical pore, we can divine the limits of the asymptotic method. The narrow width of the pore, together with the abrupt change of geometry and surface charge, leads to very strong gradients in the electric potential and the ion concentrations. These quantities can become of order ε^{-1} and start contributing to the leading order equations of (4.7a). Then, the decoupling of the fluxes into the different coordinate directions is no longer possible, requiring a full 2D model.

As the behavior of the boundary layers have huge influence on the experimentally observable quantities of the pores such as obtained current or the rectification a deep study of this effect seems be crucial.

This work might be a starting point for further investigation, especially issues such as

- the extension of the asymptotic analysis and dimension reduction to nonlinear electrolyte models for radially symmetrical geometries
- inclusion of convective transport and electro-osmotic flow inside the pore
- study the influence of big particles crossing the nanopore on the current crossing the pore. In particular, the wider spreading of charge in the solvated ions models leads to larger electro-osmotic velocities and may have a mayor impact on the processes within the pores.

References

[BAO97] I. Borukhov, D. Andelman, and H. Orland. Steric effects in electrolytes: A modified Poisson–Boltzmann equation. *Phys. Rev. Lett.*, 79:435–438, 1997.

[BD15] D. Bothe and W. Dreyer. Continuum thermodynamics of chemically reacting fluid mixtures. *Acta Mech.*, 226(6):1757–1805, 2015.

[BF00] A.J. Bard and L.R. Faulkner. *Electrochemical Methods: Fundamentals and Applications*. Wiley, New York, 2000.

[BFS14] D. Bothe, A. Fischer, and J. Saal. Global well-posedness and stability of electrokinetic flows. *SIAM J. Math. Anal.*, 46(2):1263–1316, 2014.

[Bik42] J.J. Bikerman. XXXIX. Structure and capacity of electrical double layer. *Philos. Mag.*, 33(220):384–397, 1942.

[BSW12] M. Burger, B. Schlake, and M.-T. Wolfram. Nonlinear Poisson–Nernst–Planck equations for ion flux through confined geometries. *Nonlinearity*, 25(4):961–990, 2012.

[CCAO14] J. H. Chaudhry, Jeffrey Comer, Aleksei Aksimentiev, and Luke N. Olson. A stabilized finite element method for modified Poisson–Nernst–Planck equations to determine ion flow through a nanopore. *Commun. Comput. Phys.*, 15(1):93–125, 2014.

[CGMP03] J. Cervera, V. Garcia-Morales, and J. Pellicer. Ion size effects on the electrokinetic flow in nanoporous membranes caused by concentration gradients. *J. Phys. Chem. B*, 107(33):8300–8309, 2003.

[CKC00] B. Corry, S. Kuyucak, and S.-H. Chung. Tests of continuum theories as models of ion channels. ii. Poisson–Nernst–Planck theory versus Brownian dynamics. *Biophys. J.*, 78(5):2364–2381, 2000.

[CS07] D. Constantin and Z. S. Siwy. Poisson–Nernst–Planck model of ion current rectification through a nanofluidic diode. *Phys. Rev. E*, 76:041202, 2007.

[CSP05] J. Cervera, B. Schiedt, and P.Ramirez. A Poisson/Nernst-Planck model for ionic transport through synthetic conical nanopores. *EPL*, 71(1):35, 2005.

[DGL14] W. Dreyer, C. Guhlke, and M. Landstorfer. A mixture theory of electrolytes containing solvation effects. *Electrochem. Commun.*, 43:75–78, 2014.

[DGM13] W. Dreyer, C. Guhlke, and R. Müller. Overcoming the shortcomings of the Nernst–Planck model. *Phys. Chem. Chem. Phys.*, 15:7075–7086, 2013.

[DGM15] W. Dreyer, C. Guhlke, and R. Müller. Modeling of electrochemical double layers in thermodynamic non-equilibrium. *Phys. Chem. Chem. Phys.*, 17:27176–27194, 2015.

[DGM18] W. Dreyer, C. Guhlke, and R. Müller. Bulk-surface electro-thermodynamics and applications to electrochemistry. *WIAS-Preprint*, 2511, 2018.

[FGL+18] J. Fuhrmann, C. Guhlke, A. Linke, Ch. Merdon, and R. Müller. Models and numerical methods for electrolyte flows. *WIAS-Preprint*, 2525, 2018.

[Fuh15] J. Fuhrmann. Comparison and numerical treatment of generalised Nernst–Planck models. *Comput. Phys. Comm.*, 196:166–178, 2015.

[Fuh16] J. Fuhrmann. A numerical strategy for Nernst–Planck systems with solvation effect. *Fuel cells*, 16(6):704–714, 2016.

[Gum64] H.K. Gummel. A self-consistent iterative scheme for one-dimensional steady state transistor calculations. *IEEE Trans. Electron. Dev.*, 11(10):455–465, 1964.

[HLLE12] T.-L. Horng, T.-C. Lin, C. Liu, and B. Eisenberg. PNP equations with steric effects: A model of ion flow through channels. *J. Phys. Chem. B*, 116(37):11422–11441, 2012.

[HS09] S. Howorka and Z. Siwy. Nanopore analytics: sensing of single molecules. *Chem. Soc. Rev.*, 38:2360–2384, 2009.

[Hun13] R. J. Hunter. *Zeta potential in colloid science: principles and applications*, volume 2. Academic press, 2013.

[JF+18] T. Streckenbach J. Fuhrmann et al. pdelib. `http://pdelib.org`, 2018.

[KBA07] M. S. Kilic, M. Z. Bazant, and A. Ajdari. Steric effects in the dynamics of electrolytes at large applied voltages. II. Modified Poisson-Nernst-Planck equations. *Phys. Rev. E*, 75:021503, 2007.

[Key11] U.F. Keyser. Controlling molecular transport through nanopores. *J. R. Soc. Interface*, 8(63), 2011.

[MPWR18] B. Matejczyk, J.-F. Pietschmann, M.-T. Wolfram, and G. Richardson. Asymptotic models for transport in large aspect ratio nanopores. *Eur. J. Appl. Math.*, pages 1–28, 2018.

[Mül85] I. Müller. *Thermodynamics*. Pitman Publishing, London, 1985.

[NTA04] J. Newman and K.E. Thomas-Alyea. *Electrochemical Systems*. Wiley, Hoboken, NJ, 2004.

[PWB+13] J.-F. Pietschmann, M.-T. Wolfram, M. Burger, C. Trautmann, G. Nguyen, M. Pevarnik, V. Bayer, and Z. Siwy. Rectification properties of conically shaped nanopores: consequences of miniaturization. *Phys. Chem. Chem. Phys.*, 15:16917–16926, 2013.

[SAB+03] Z. Siwy, P. Apel, D. Baur, D.D. Dobrev, Y.E. Korchev, R. Neumann, R. Spohr, C. Trautmann, and K.O. Voss. Preparation of synthetic nanopores with transport properties analogous to biological channels. *Surf. Sci.*, 532:1061–1066, 2003.

[Sch97] J. Schöberl. NETGEN An advancing front 2D/3D-mesh generator based on abstract rules. *Computing and visualization in science*, 1(1):41–52, 1997.

[SG69] D.L. Scharfetter and H.K. Gummel. Large-signal analysis of a silicon Read diode oscillator. *IEEE Trans. Electron. Dev.*, 16(1):64–77, 1969.

[SGNE08] A. Singer, D. Gillespie, J. Norbury, and R. S. Eisenberg. Singular perturbation analysis of the steady-state Poisson–Nernst–Planck system: Applications to ion channels. *Eur. J. Appl. Math.*, 19(5):541–560, 2008.

[SN09] A. Singer and J. Norbury. A Poisson–Nernst–Planck model for biological ion channels – an asymptotic analysis in a three-dimensional narrow funnel. *SIAM J. Appl. Math.*, 70(3):949–968, 2009.

[VSS08] I. Vlassiouk, S. Smirnov, and Z. Siwy. Ionic selectivity of single nanochannels. *Nano Lett.*, 8(7):1978–1985, 2008.

[YVS+05] Z. Yang, T. A. Van, D. Straaten, U. Ravaioli, and Y. Liu. A coupled 3-d PNP/ECP model for ion transport in biological ion channels. *J. Comput. Electron.*, 4(1):167–170, 2005.

[ZW11] Q. Zheng and G.-W. Wei. Poisson–Boltzmann–Nernst–Planck model. *J. Chem. Phys.*, 134(19):194101, 2011.